Title
Comparison of water and lipid content measurements using diffuse optical spectroscopy and MRI in emulsion phantoms.

Journal
Technology in cancer research & treatment, 2(6)

ISSN
1533-0346

Authors
Merritt, S
Gulsen, G
Chiou, G
et al.

Publication Date
2003-12-01

DOI
10.1177/153303460300200608

Technology in Cancer Research & Treatment
ISSN 1533-0346
Volume 2, Number 6, December (2003)

Comparison of Water and Lipid Content Measurements Using Diffuse Optical Spectroscopy and MRI in Emulsion Phantoms

www.tcrt.org

Sean Merritt, B.S.[1]
Gultekin Gulsen, Ph.D.[2]
George Chiou, Ph.D.[2]
Yong Chu, B.S.[2]
Chengwu Deng, B.S.[2]
Albert E. Cerussi, Ph.D.[1]
Anthony J. Durkin, Ph.D.[1]
Bruce J. Tromberg, Ph.D.[1,*]
Orhan Nalcioglu, Ph.D.[2]

[1]Laser Microbean and Medical Program
Beckman Laser Institute
University of California Irvine
Irvine, California 92612, USA
[2]John Tu and Thomas Yuen Center for
Functional Onco-Imaging
University of California Irvine
Irvine, California 92697, USA

We present a quantitative comparison of lipid and water signals obtained from broadband Diffuse Optical Spectroscopy (DOS) and Magnetic Resonance Imaging (MRI). DOS and MRI measurements were performed on an identical set of emulsion phantoms that were composed of different water/soybean oil fractions. Absolute concentrations of water and lipid ranging from 35-94% and 63-6%, respectively were calculated from quantitative broadband near-infrared (NIR) absorption spectra (650-1000 nm). MR images of fat and water were separated using the three-point Dixon technique. DOS and MRI measured water and lipid were highly correlated (R^2 = 0.98 and R^2 = 0.99, respectively) suggesting that these techniques are complementary over a broad range of physiologically relevant water and lipid values. In addition, comparison of DOS derived concentrations to the MRI "gold standard" technique validates our quantitation approach and permits estimation of DOS accuracy and sensitivity *in vivo*.

Key words: Optical, Spectroscopy, NRI, MRI.

Introduction

The development of non-invasive diagnostic techniques to image and characterize physiological properties of tissues is an area of intense research and clinical interest. Magnetic resonance imaging (MRI) and near-infrared diffuse optical spectroscopy (DOS) are non-invasive techniques that provide complementary structural and functional physiological information. DOS can be used to measure chromophore concentrations such as oxy- and dexoy-hemoglobin ($Hb0_2$ and Hb-R, respectively), water and fat within a local volume of tissue, whereas MRI provides high-resolution structural and contrast-enhanced images. Co-registration of these two methods has the potential to enhance our understanding of the complex biological processes associated with tumor transformation and growth. Ultimately, the combination of the two measurement techniques can be applied to monitoring tumor changes in response to therapy, resulting in an improved method to test cancer treatment efficacy (1, 2).

The integration of DOS with MRI has particular promise in breast cancer characterization and detection. MRI can provide excellent anatomical resolution and is used widely in breast cancer research with exogenous probes to enhance tumor/normal tissue contrast (2-7). Compared to MRI, DOS is still in an early developmental stage and its utility is currently being evaluated as a breast cancer diagnostic or monitoring tool (8-13). The attributes of DOS that would strengthen current MRI systems are that DOS provides an absolute measure of HbO_2 and HB-R and also provides a higher contrast between normal breast tissue and tumor tissue than MRI.

* Corresponding Author:
Bruce J. Tromberg, Ph.D.
Email: Tromberg@bli.uci.edu

Few DOS studies have directly measured or accounted for water and lipid in breast, the principal endogenous contrast elements in MR images. This is particularly important because the accuracies of HbO_2 and HB-R quantitation in breast tissue are strongly dependent on assumptions regarding H_2O and lipid. Some researchers have fixed H_2O and lipid to population averaged values (9) however recent studies underscore the importance of direct H_2O/lipid quantitation since these parameters can vary substantially in both normal breast and tumors (8, 12, 13). For example, in a previous study we utilized a broadband DOS instrument to monitor breast tumors as patients underwent neoadjuvant chemotherapy treatment (1). We observed a 4.4-fold decrease in the water/lipid ratio over 3 chemotherapy cycles (68 days) and a 34% reduction in water content within only five days of the first treatment. McBride *et al*. used a 16 source, 16 detector Diffuse Optical Tomography instrument to collect and reconstruct optical images of breast tumors *in vivo* (9). This study compared a variety of computational techniques used to compensate for water and lipid content in optical hemoglobin images of the breast. They concluded that prior knowledge of these parameters would significantly improve the accuracy of HbO_2 and Hb-R image reconstruction. Piferri *et al*. recently introduced a four wavelength optical mammography scanner that utilized lasers at wavelengths at 912 nm and 975 nm, giving the instrument sensitivity to water and lipid content within the breast (11).

There have only been a few reports of the combination of DOS and MRI in breast cancer studies (14-19). Ntziachristos *et al*. developed a diffuse optical imaging instrument for co-registration with MRI (14, 15). Their optical system acquires time-resolved data at up to three wavelengths in the near infrared region, and they have reported the first clinical application of MR-guided DOS to breast measurements (16). Another combined system has been used by our group to co-register DOS measurements with MR images in a rat tumor model (17-19). In these studies we reported a qualitative correlation between DOS measurements of H_2O, hemoglobin, and optical contrast agents and MRI measurements of tumor viability, edema, and necrosis.

The necessary next step to these studies is a more quantitative correlation of DOS and MRI signals derived from identical tissue structures. There are two components of tissue that produce a signal measurable by both modalities: water and lipids. MRI has multiple techniques of chemical shift imaging, which is able to separate water and fat images by utilizing the different resonant frequencies of the protons in the hydrogen of water and fat molecules (20-23). DOS also has the ability to measure water and lipids *in vivo* through its sensitivity to the near-infrared vibrational overtones of the water O-H bond (978 nm) and lipid C-H bonds (930 nm) (24, 25).

In this paper we present results from an investigation of the correlation between MRI and DOS data obtained from water and soybean oil emulsion phantoms. DOS measured water and lipid concentrations are compared with calibrated MRI water and fat images providing a quantitative comparison of measurements by each technique. Our results show excellent agreement between the developing DOS technology and the established technology of MRI for both water and lipid measurements. This work provides validation of the accuracy and sensitivity of DOS measurements *in vivo* through a quantitative comparison with the medical imaging "gold standard" of MRI.

Materials and Methods

Diffuse Optical Spectroscopy

Instrumentation: We used a combined frequency-domain (FD) and steady-state (SS) system that has previously been described in detail (26). At the core of the frequency-domain instrument is a network analyzer (HP 8753D), that is used to modulate the intensity of diode lasers, and to measure the phase and amplitude of the diffusely reflected optical signal detected by an avalanche photodiode (Hamamatsu APD C556P-56045-03). Six diode lasers at wavelengths of 661, 681, 783, 806, 823 and 850 nm are intensity modulated from 50 to 500 Mhz sweeping a total of 294 frequencies. The SS instrument is composed of a tungsten-halogen light source (Ocean Optics LS-1) and a spectrometer (Oriel MS127i, InstraSpec IV CCD). As explained in the next section, the combination of FD and SS data allows for the determination of broadband absorption and scattering spectra of the tissue (typically 650-1000 nm).

The FD and SS light were delivered to the sample through optical fibers that were secured in a Delrin probe. Two detection fibers for the FD and SS measurement were each fixed in the probe at a distance of 6 mm from their corresponding source fiber.

For the FD measurements, amplitude and phase were calibrated using a liquid phantom consisting of two parts Lyposyn 10% IV (LOT 05-372-DE) with one part water. The optical properties of the calibration phantom were determined prior to the sample measurements through a set of multi-frequency, multi-distance, infinite geometry measurements (27). For the SS measurements, an integrating sphere was used to calibrate the spectral instrument response.

DOS Analysis: The method used to determine the optical properties is explained in detail by Bevilaqua *et al*. (26). The computations are based on the analytical diffusion solution of the reflectance $R(\mu_a(\lambda),\mu_s'(\lambda), f)$ given by Kienle and Patterson, where $\mu_a(\lambda)$ is the absorption coefficient, $\mu_s'(\lambda)$ the reduced scattering coefficient, and f the modulation fre-

quency (28). The same analytical solution is valid for steady-state (f=0) and frequency-domain data (26). First, $\mu_a(\lambda)$ and $\mu_s'(\lambda)$ are obtained at the laser diode wavelengths from the fit of the diffusion solution to the calibrated phase and amplitude of the light that is measured at the tissue surface. Assuming μ_s' to have the form, $\mu_s'(\lambda) = A \cdot \lambda^{-B}$, the broadband scattering spectrum can be obtained by fitting the $\mu_s'(\lambda)$ values at the laser diode wavelengths to the above equation (29-31). The $\mu_a(\lambda)$ and $\mu_s'(\lambda)$ values at the laser wavelengths obtained from FD measurements are also used to calibrate the broadband reflectance spectrum obtained from SS measurements, again using diffusion theory. Note that this calibration step corresponds only to the determination of a single scaling factor that allows for the determination of the absolute reflectance spectrum $R(\lambda)$ expressed in [w/m^2]. The last step is to determine the broadband absorption spectra $\mu_a(\lambda)$ from the broadband absolute reflectance spectra $R(\lambda)$ and the broadband $\mu_s'(\lambda)$ spectrum, using the diffusion equation solution a third time. Finally, chromophore concentrations are determined by a linear least-squares fit of the absorption spectra of the chromophores to the measured absorption spectrum over the 650-1000 nm wavelength range. When used to measure tissue *in vivo* the parameters that are extracted from the chromophore fit include HbO_2, Hb-R, H_2O and lipid content. In this study, the parameters extracted from the set of phantoms include H_2O and lipids.

MRI Instrument and Methodology: The MRI system is a homebuilt 4T scanner with a Philips Medical, Inc. EDGE console. The bore diameter is 90 cm, and a birdcage-type transmit-receive RF coil is utilized for the studies. The three-point Dixon (3PD) technique is applied for determination of water and fat concentrations (21, 22). In conventional quantitative MR images of these phantoms, the signal within a voxel is the vector sum of the fat and water signals of the protons within that voxel. The 3PD technique separates the MR signal into the individual contributions of fat and water in each voxel of tissue, therefore, the fat and water fractions can be calculated. Fat and water protons resonate at slightly different frequencies and fall alternatively in and out of phase with each other at a certain magnetic field by selecting appropriate pulse sequence parameters (20).

Coronal images of the water/fat emulsion phantoms were obtained utilizing fast spin-echo sequence with TR = 5000ms, TE = 15ms, field of view (FOV) = 15cm, 128 × 128 matrix, and a slice thickness of 3 mm. Nine test tubes that spanned the range from 3-94% water and 65-6% lipid by volume were placed in a holder. This holder was placed in the RF coil with two additional test tubes containing pure water and pure soybean oil.

The images were analyzed with custom-developed MATLAB-based tools that apply the 3PD technique to fat/water phase shifts of $-\pi$, 0, and π radians. As a result we are able to accurately separate the MR images into fat and water components. A circular ROI covering 70% of the cross-section was placed on each phantom. The fat and water contents were determined by comparing the mean ROI intensity of each phantom with the mean intensity measured from pure water and pure soybean oil phantoms. The error bars presented are given by the standard deviation of the individual pixel intensities that were enclosed within the ROI of interest.

Emulsion Phantom Study: An emulsion phantom set was made to simulate tissues composed of different water/lipid ratios. The composition of the phantoms included water, soybean oil and Triton x-100. The water and soybean oil provide the same absorption characteristics as water and lipids in breast tissue. Triton x-100 is an emulsifying agent that was added to each phantom in the amount of 4 percent of the volume of the oil. The NIR absorption spectrum of Triton x-100 has features that are similar to soybean oil. Because the Triton x-100 accounted for only 0.4-2.2% of the emulsion volumes, we excluded its contribution from the chromophore fit (see DOS Analysis section).

The phantoms were made by combining the soybean oil with Triton x-100 and heating to 60ºC until the Triton x-100 had dissolved in the oil (~10 min). The water was placed in a household blender and the soybean oil mixture was added and blended on the highest speed for 1 minute. The emulsion was then poured into a separate container and placed in a vacuum chamber that was connected to an in-house vacuum system. Each phantom was left under vacuum for one hour in order to remove air bubbles from the mixture. A set of twelve 0.5 L phantoms were prepared and measured by DOS with water (lipid) composition ranging from 35 to 94 (65 to 6) percent by volume (Table I). A small amount (~10 ml) was removed from nine of these emulsions for MRI measurements.

Table I
Composition of emulsion phantoms.

Phantom #	H2O [% volume]	Soybean oil [% volume]	Triton x-100 [% volume]
1	69.4	29.5	1.1
2	60.0	38.5	1.5
3	48.9	49.1	2
4	41.2	57.1	1.7
5	84.9	14.4	0.7
6	73.5	25.3	1.2
7	63.9	34.8	1.3
8	34.6	63.2	2.2
9	94.1	5.5	0.4
10	88.7	10.7	0.6
11	78.6	20.5	0.9
12	53.9	44.1	1.9

DOS measurements were performed by placing the optical probe at the surface of the emulsion phantom. Three successive measurements were obtained from each phantom with stirring between measurements to ensure homogeneity and

adequate volume sampling. The DOS values presented are an average of the three measurements and the error bars represent the standard deviation of the multiple measurements.

Results and Discussion

Figure 1 shows a typical μ_a spectrum obtained from phantom #4, using the combined frequency-domain and steady-state measurements explained in the DOS Analysis section. The peak absorption features of soybean oil at 930 nm and H_20 at 978 nm are in excellent agreement with previously reported results (8, 12, 26). The fit of the chromophore spectra (H_2O, lipid and a constant background absorption) to the μ_a spectrum allows for the determination of water and lipid content. The background absorption is less than 8% of the absorption value at 930nm (lipid peak) for all phantom measurements. The background absorption serves to correct for a systematic offset in the absorption value due to both transport model and calibration inaccuracy. Previous studies in tissue phantoms have shown that, in the case of a broadband absorption spectrum, adding this degree of freedom in the fit can significantly improve its accuracy (32).

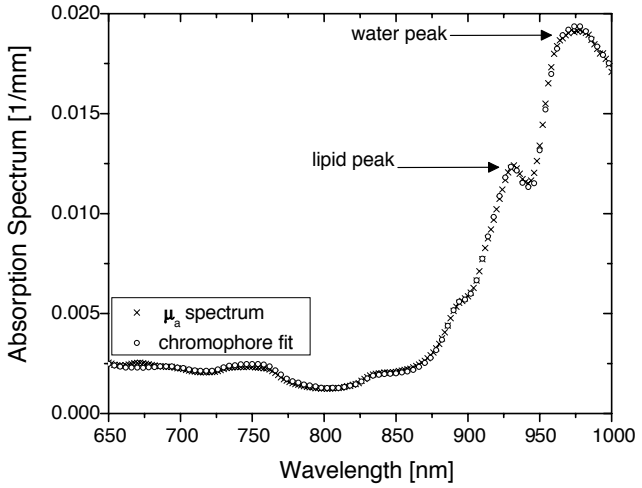

Figure 1: Measured absorption spectrum for phantom 4.

Figure 2 shows the fat and water MR images of the emulsion phantoms. The left most images is the combined water and lipid signals, the middle image is the water only signal and the right image is the lipid only signal.

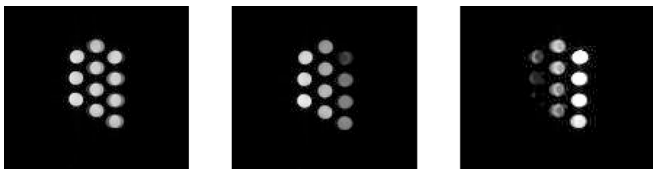

Figure 2: In-phase MR image showing both lipid and water (left), water image (middle) and fat image (right). The pure water sample is in the lower left-hand corner and pure soybean oil is in the upper right hand corner. The phantoms from Table I shown in the images are phantoms # 9, 5, 6, 1, 7, 2, 3, 4, and 8 in order of decreasing water.

Figures 3 and 4 show how the DOS and MRI measured water and lipid volume [%] compare with expected values. In general, both figures demonstrate that there is a strong correlation between actual and measured values. One apparent difference between DOS and MRI is that the MRI data appear to correlate better with the true phantom composition, particularly in the case of lipid measurements. This is due to the fact that the MRI phantom measurements are calibrated with pure water and soybean oil, which constrains the relative values to the expected line. DOS uses spectra derived from pure water and soybean oil in the chromophore fit, but does not use measurements from pure samples during data acquisition to calibrate the system. In order for DOS to perform a calibration in the same manner as the MRI, it would have to measure a turbid sample of pure water and pure soybean oil and use these measurements to normalize the recovered values. This could be done with pure water by adding microspheres, but to our knowledge there are no solids that can be suspended in soybean oil to create a uniform, turbid sample.

In Figure 3, the water is consistently underestimated by DOS, while the MRI measurements are distributed evenly. The line of DOS measurements is tighter than the MRI measurements, except for phantom #11, which stands out as an anomalous point. Although there is a large error in the DOS water value recovered for phantom 11, the lipid value is consistent with the other phantom measurements. The anomalous water value recovered for phantom #11 is likely due to air bubbles in the phantom that were near the source or detector fibers. During the process of perfecting the properties of the phantoms, we found that a visual increase in the number of air bubbles in the phantoms correlated with increased errors in the phase and amplitude fits of the light that had propagated through the sample. Phantoms #11 was the only phantom that showed any deviation in the phase and amplitude fits, which is consistent with the error in the water measured.

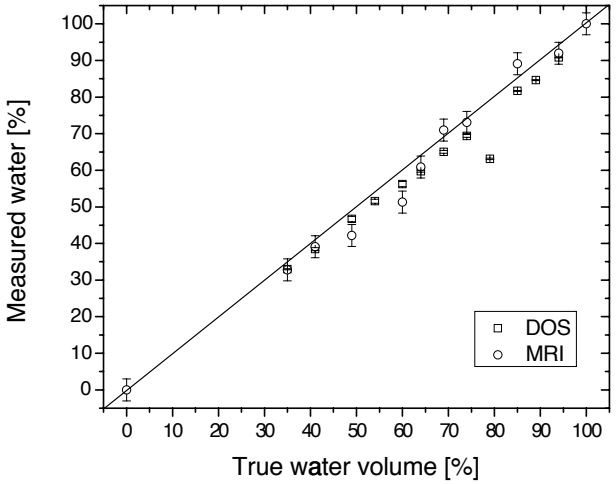

Figure 3: Measured water vs. true water for DOS and MRI.

Although this water value measured was not correct, the error bars for the measurement are small, which is more a description of the precision of the DOS measurement rather than the accuracy as compared to the true value. Phantom #11 was measured five days later with more care taken to eliminate possible air bubbles and the water value measured was 81 percent, which is very near the true water value.

In Figure 4 the lipid content is consistently overestimated by DOS. If the point for phantom 11 is neglected and a linear fit is performed for the two DOS plots, they provide trend-lines that are very nearly parallel to the expected "true value" line. The water trend-line passes within 2% of zero at the y-intercept, but the trend-line for the recovered lipids crosses the y-axis at 9% and remains shifted with a 9% constant offset from the expected lipid values. This offset of the fat from the expected value is most likely due to errors in the estimation of extinction coefficient of soybean oil that is implemented in the chromophore fit. A contribution to the offset is most likely also derived from the surfactant in the phantoms, which has an absorption profile similar to soybean oil but is neglected in the chromophore fit because of the small concentrations used. Although, these effects could account for a small overestimation of lipid values, DOS lipid measurements are clearly linear with a consistent offset over a broad dynamic range. The correlation coefficients for the DOS and MRI trend-lines (including phantom 11) are: DOS water $R^2 = 0.96$, DOS lipids $R^2 = 1.00$, MRI water $R^2 = 0.99$ and MRI lipids $R^2 = 1.00$.

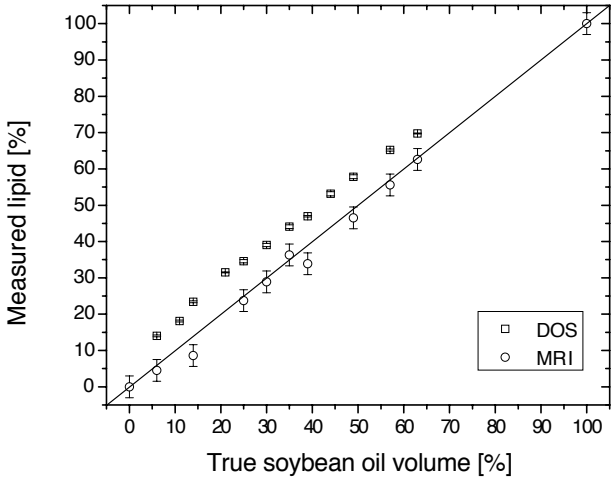

Figure 4: Measured lipid vs. true soybean oil for DOS and MRI.

Lastly, Figures 5 and 6 provide a direct comparison between DOS measurements and MRI for water and fat, respectively. The correlations are excellent ($R^2_{water} = 0.98$ and $R^2_{lipid} = 0.99$) suggesting that optical and MRI signals are derived from identical phantom components. In addition, by comparing DOS results to the MRI "gold standard", we further validate DOS as a quantitative technique for lipid and water analysis in tissue.

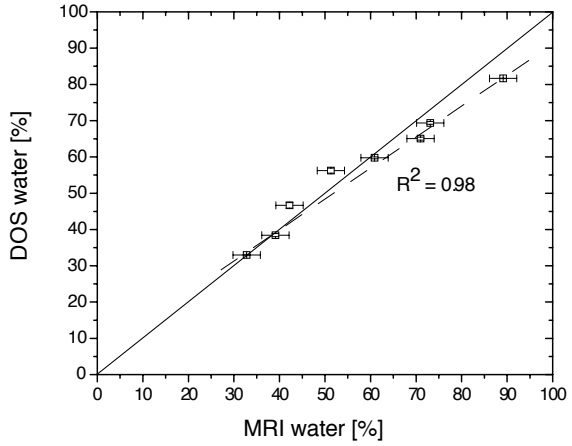

Figure 5: DOS water vs. MRI water.

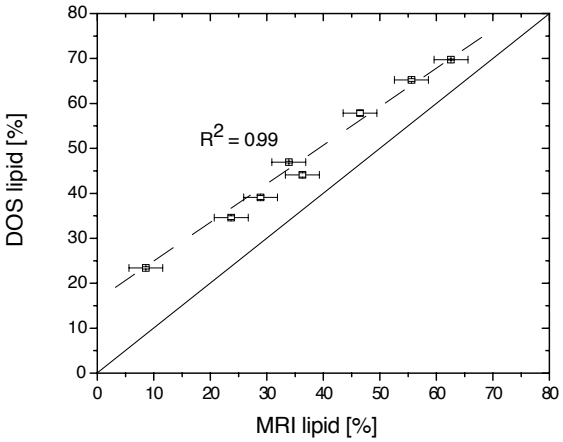

Figure 6: DOS lipid vs. MRI lipid.

Conclusions

To the best of our knowledge this is the first report of a quantitative comparison between MRI and DOS. In practical terms, this work could lead to improvements in both MRI and DOT image analysis.

For example, Pogue *et al*. (33) proposed to use *a priori* information from MR images to constrain the image reconstruction of DOT. Using this approach, the optical inverse problem can be simplified by constraining boundaries on optical images of water and lipid based on water and fat MR images. The resulting image would be higher resolution than DOT could offer independently and the functional information would be absolute and provide higher contrast than MRI. In addition, an absolute MRI measurement of water and fat concentrations *in vivo* (34, 35) could be used to constrain optical images of total hemoglobin and tissue oxygen saturation for more accurate results in optical systems with low spectral content.

Acknowledgements

This work was supported by the National Institutes of Health under grants (Laser Microbeam and Medical Program: LAMMP) and NIH P20-CA86182, and the Air Force Office of Scientific Research (AFOSR F49620-00-1-0371). SM acknowledges the California Breast Cancer Research Program for fellowship support.

References

1. D. Jakubowski, A. E. Cerussi, F. Bevilacqua, N. Shah, D. Hsiang, J. Butler and B. J. Tromberg. Monitoring Neoadjuvant Chemotherapy in Breast Cancer using Quantitative Diffuse Optical Spectroscopy: A Case Study. *J. Biomed. Opt.* (2004).
2. N. R. Jagannathan, M. Singh, V. Govindaraju, P. Raghunathan, O. Coshic, P. K. Julka and G. K. Rath. Volume Localized *In Vivo* Proton MR Spectroscopy of Breast Carcinoma: Variation of Water-fat Ratio in Patients Receiving Chemotherapy. *NMR Biomed. 11*, 414-422 (1998).
3. B. L. Daniel, K. Butts, G. H. Glover, C. Cooper and R. J. Herfkens. Breast Cancer: Gadolinium-enhanced MR Imaging with a 0.5-T Open Imager and Three-point Dixon Technique. *Radiology 207*, 183-190 (1998).
4. W. Du, Y. P. Du, U. Bick, X. Fan, P. M. MacEneaney, M. A. Zamora, M. Medved and G. S. Karczmar. Breast MR Imaging with High Spectral and Spatial Resolutions: Preliminary Experience. *Radiology 224*, 577-585 (2002).
5. M. Hirose, D. F. Kacher, D. N. Smith, C. M. Kaelin and F. A. Jolesz. Feasibility of MR Imaging-guided Breast Lumpectomy for Malignant Tumors in a 0.5-T Open-configuration MR Imaging System. *Acad. Radiol. 9*, 933-941 (2002).
6. S. G. Orel and M. D. Schnall. MR Imaging of the Breast for the Detection, Diagnosis, and Staging of Breast Cancer. *Radiology 220*, 13-30 (2001).
7. M. D. Schnall. Breast MR Imaging. *Radiol Clin North Am 41*, 43-50 (2003).
8. A. E. Cerussi, D. Jakubowski, N. Shah, F. Bevilacqua, R. Lanning, A. J. Berger, D. Hsiang, J. Butler, R. F. Holcombe and B. J. Tromberg. Spectroscopy Enhances the Information Content of Optical Mammography. *J. Biomed. Opt. 7*, 60-71 (2002).
9. T. O. McBride, B. W. Pogue, S. Poplack, S. Soho, W. A. Wells, S. Jiang, U. L. Osterberg and K. D. Paulsen. Multispectral Near-infrared Tomography: A Case Study in Compensating for Water and Lipid Content in Hemoglobin Imaging of the Breast. *J. Biomed. Opt. 7*, 72-79 (2002).
10. D. Jakubowski, A. E. Cerussi, F. Bevilacqua, N. Shah, D. Hsiang, J. Butler and B. J. Tromberg. Monitoring Neoadjuvant Chemotherapy in Breast Cancer using Quantitative Diffuse Optical Spectroscopy: A Case Study. *J. Biomed. Opt.* (2003).
11. A. Pifferi, P. Taroni, A. Torricelli, F. Messina, R. Cubeddu and G. Danesini. Four-wavelength Time-resolved Optical Mammography in the 680-980-nm Range. *Opt. Lett. 28*, 1138-1140 (2003).
12. A. E. Cerussi, A. J. Berger, F. Bevilacqua, N. Shah, D. Jakubowski, J. Butler, R. F. Holcombe and B. J. Tromberg. Sources of Absorption and Scattering Contrast for Near-infrared Optical Mammography. *Acad. Radiol. 8*, 211-218 (2001).
13. R. Cubeddu, C. D'Andrea, A. Pifferi, P. Taroni, A. Torricelli and G. Valentini. Effects of the Menstrual Cycle on the Red and Near-infrared Optical Properties of the Human Breast. *Photochem. Photobiol. 72*, 383-391 (2000).
14. V. Ntziachristos, A. H. Hielscher, A. G. Yodh and B. Chance. Diffuse Optical Tomography of Highly Heterogeneous Media. *IEEE Trans. Med. Imaging. 20*, 470-478 (2001).
15. V. Ntziachristos, A. G. Yodh, M. Schnall and B. Chance. Concurrent MRI and Diffuse Optical Tomography of Breast After Indocyanine Green Enhancement. *Proc. Natl. Acad. Sci. USA 97*, 2767-2772 (2000).
16. V. Ntziachristos, A. G. Yodh, M. D. Schnall and B. Chance. MRI-guided Diffuse Optical Spectroscopy of Malignant and Benign Breast Lesions. *Neoplasia 4*, 347-354 (2002).
17. S. Merritt, F. Bevilacqua, A. J. Durkin, D. J. Cuccia, R. Lanning, B. J. Tromberg, G. Gulsen, H. Yu, J. Wang and O. Nalcioglu. Coregistration of Diffuse Optical Spectroscopy and Magnetic Resonance Imaging in a Rat Tumor Model. *Appl. Opt. 42*, 2951-2959 (2003).
18. G. Gulsen, H. Yu, J. Wang, O. Nalcioglu, S. Merritt, F. Bevilacqua, A. J. Durkin, D. J. Cuccia, R. Lanning and B. J. Tromberg. Congruent MRI and Near-infrared Spectroscopy for Functional and Structural Imaging of Tumors. *Technol. Cancer Res. Treat. 1*, 497-505 (2002).
19. D. J. Cuccia, F. Bevilacqua, A. J. Durkin, S. Merritt, B. J. Tromberg, G. Gulsen, H. Yu, J. Wang and O. Nalcioglu. *In Vivo* Quantification of Optical Contrast Agent Dynamics in Rat Tumors by Use of Diffuse Optical Spectroscopy with Magnetic Resonance Imaging Coregistration. *Appl. Opt. 42*, 2940-2950 (2003).
20. W. T. Dixon. Simple Proton Spectroscopic Imaging. *Radiology 153*, 189-194 (1984).
21. G. H. Glover and E. Schneider. Three-point Dixon Technique for True Water/Fat Decomposition with B0 Inhomogeneity Correction. *Magn. Reson. Med. 18*, 371-383 (1991).
22. P. A. Hardy, R. S. Hinks and J. A. Tkach. Separation of Fat and Water in Fast Spin-echo MR Imaging with the Three-point Dixon Technique. *J. Magn. Reson. Imaging 5*, 181-185 (1995).
23. J. H. Simon and J. Szumowski. Proton (Fat/Water) Chemical Shift Imaging in Medical Magnetic Resonance Imaging. Current Status. *Invest. Radiol. 27*, 865-874 (1992).
24. R. T. Holeman and P. R. Edmondson. Near-Infrared Spectra of Fatty Acids and Some Related Substances. *Analytical Chemistry 28*, 1533-1538 (1956).
25. L. G. Weyer. Near-Infrared Spectroscopy of Organic-Substances. *Applied Spectroscopy Reviews 21*, 1-43 (1985).
26. F. Bevilacqua, A. J. Berger, A. E. Cerussi, D. Jakubowski and B. J. Tromberg. Broadband Absorption Spectroscopy in Turbid Media by Combined Frequency-domain and Steady-state Methods. *Applied Optics 39*, 6498-6507 (2000).
27. T. H. Pham, O. Coquoz, J. B. Fishkin, E. Anderson and B. J. Tromberg. Broad Bandwidth Frequency Domain Instrument for Quantitative Tissue Optical Spectroscopy. *Review of Scientific Instruments 71*, 2500-2513 (2000).
28. A. Kienle and M. S. Patterson. Improved Solutions of the Steady-state and the Time-resolved Diffusion Equations for Reflectance from a Semi-infinite Turbid Medium. *Journal of the Optical Society of America a-Optics Image Science and Vision 14*, 246-254 (1997).
29. R. Graaff, J. G. Aarnoudse, J. R. Zijp, P. M. A. Sloot, F. F. M. Demul, J. Greve and M. H. Koelink. Reduced Light-Scattering Properties for Mixtures of Spherical-Particles – A Simple Approximation Derived from Mie Calculations. *Applied Optics 31*, 1370-1376 (1992).
30. J. M. Schmitt and G. Kumar. Optical Scattering Properties of Soft Tissue: A Discrete Particle Model. *Applied Optics 37*, 2788-2797 (1998).
31. J. R. Mourant, J. P. Freyer, A. H. Hielscher, A. A. Eick, D. Shen and T. M. Johnson. Mechanisms of Light Scattering from Biological Cells Relevant to Noninvasive Optical-tissue Diagnostics. *Applied Optics 37*, 3586-3593 (1998).
32. D. Jakubowski. Development of Broadband Quantitative Tissue Optical Spectroscopy for the Non-invasive Characterization of Breast Disease. Ph. D. Dissertation (University of California, Irvine, Irvine, 2002).
33. B. W. Pogue and K. D. Paulsen. High-resolution Near-infrared Tomographic Imaging Simulations of the Rat Cranium by Use of *A Priori* Magnetic Resonance Imaging Structural Information. *Optics Letters 23*, 1716-1718 (1998).

34. R. Ross, B. Goodpaster, D. Kelley and F. Boada. Magnetic Resonance Imaging in Human Body Composition Research – From Quantitative to Qualitative Tissue Measurement. *In Vivo Body Composition Studies 904*, 12-17 (2000).

35. F. Boada, R. Ross, V. A. Stenger, D. C. Noll, B. Goodpaster and D. Kelley. Absolute Quantitation of Skeletal Muscle Lipid Content with MRI. *Scientific Meeting International Society for Magnetic Resonance in Medicine*. 21-51. Philadelphia.

Date Received: October 2, 2003